Circular Switching Surface Technique: High-Performance Constant Power Load Stabilization for Electric Vehicle Systems

Matias Anun, *Member, IEEE*, Martin Ordonez, *Member, IEEE*, Ignacio Galiano Zurbriggen, *Student Member, IEEE*, and German G. Oggier, *Member, IEEE*

***Abstract*—Electric vehicles make use of energy storage systems, such as batteries and/or ultracapacitors to power the electric power drive train, as well as auxiliary automotive system for control, safety, and comfort. This relatively complex power structure can be described as a distributed multiconverter system. The constant power behavior of tight-speed controllers in the vehicle's traction system and tightly regulated dc–dc converters connected to the HV-DC bus produces instability effects. This paper proposes a simple and practical geometric control, using circular switching surfaces, to address constant power load instability in electric vehicle's power systems. The proposed switching surfaces provide a solution in the geometrical domain to constant power loading conditions, while achieving outstanding dynamic response compared to state-of-the-art controllers. The controller is implemented in a bidirectional Buck + Boost cascade converter as a battery charge/discharge unit and ensures reliable system operation. The predictable and consistent behavior of the converter with constant power load is presented by analyzing the system curves in the normalized state plane with the switching surfaces employed. Simulation and experimental results on a scaled 1-kW Buck + Boost cascade converter validate the proposed switching surfaces and predictions regarding the converter's behavior under constant power loading conditions.**

***Index Terms*—Battery management systems, boundary control, circular switching surfaces (CSS), constant power load (CPL), dc-link capacitance, dc–dc power converters, electric vehicles (EVs).**

I. Introduction

THE development of sustainable transport system has experienced great improvements in the last 15 years. As a result, electric vehicles (EVs) namely hybrid electric vehicles (HEVs) and all-electric or battery electric vehicles (BEVs) are slowly starting to coexist with regular internal combustion vehicles around the world. In advanced automotive structures, besides the electric propulsion system, several electrical subsystems are used for control, safety, and comfort in the vehicle. The relatively complex power structure of automotive electric systems can be described as a distributed multiconverter scheme including dc as well as ac subsystems [1]–[3]. A simplified block diagram of the distributed system of a BEV is illustrated in Fig. 1(a), where the main dc bus feeds the electric motor drive and downstream converters, which power different automotive electric subsystems.

EVs are propelled using bidirectional dc–dc converters as battery charge/discharge units (BCDUs) that interface energy storage systems such as batteries and ultracapacitors with the main dc bus [4]. These converters are suitable for controlling power flow in motoring and regenerative braking operation to improve the overall system efficiency and travel range. The dc-link voltage is typically higher than the energy storage voltage; thus, step-up operation is required to obtain the dc-link voltage level [5]. However, in cases where the nominal battery output voltage, which depends mainly on the number of cell stacked, overlaps with the dc-link voltage required by the propulsion system, step-down operation is necessary as well [6]. The Buck + Boost cascade converter depicted in the lower part of Fig. 1(a) is capable of performing step-down and step-up operations and presents enhanced properties such as increased performance and efficiency in comparison to other bidirectional dc–dc converters [7]–[10].

Power converters fed by the main bus create unique dynamic characteristics that have been the subject of study over the past few years. Under tight-speed regulation with constant torque-load relationship, the motor drive exhibits constant power (CP) behavior at the input of dc bus [11], [12]. A similar situation occurs in downstream converters under tight regulation [13]–[17]. As shown in [13], the dynamic behavior of constant power loads (CPLs) is equivalent to a dynamic negative resistance which, under certain conditions, can produce instability in the dc bus and consequently, in the system. Limitations of practical CPLs in real-world application have been assessed in [14]. However, in this study, an ideal model (infinite bandwidth) of the CPL is employed in the analysis to account for the worst-case scenario. If stability and high performance is achieved for the theoretical CPL (infinite bandwidth), then stable operation and fast response is guaranteed for any other CPL case (e.g., high-bandwidth and low-bandwidth CPLs). From the practical point of view, it is not possible to accomplish ideal CPL behavior. Nevertheless, a very high-bandwidth CPL is

Manuscript received December 10, 2013; revised August 12, 2014; accepted September 6, 2014. Date of publication September 17, 2014; date of current version March 5, 2015. This work was supported by the Natural Sciences and Engineering Research Council, Canada. Recommended for publication by Associate Editor G. Escobar.

M. Anun, M. Ordonez, and I. Galiano Zurbriggen are with the Department of Electrical and Computer Engineering, University of British Columbia, Vancouver, BC V6T 1Z4 Canada (e-mail: manun@ieee.org; mordonez@ieee.org; igaliano@ieee.org).

G. G. Oggier is with the Department of Electrical and Computer Engineering, University of British Columbia, Vancouver, BC V6T 1Z4 Canada, and also with the Consejo Nacional de Investigaciones Cientificas y Tecnicas, 1917 Buenos Aires, Argentina (e-mail: goggier@ieee.org).

Color versions of one or more of the figures in this paper are available online at http://ieeexplore.ieee.org.

Digital Object Identifier 10.1109/TPEL.2014.2358259

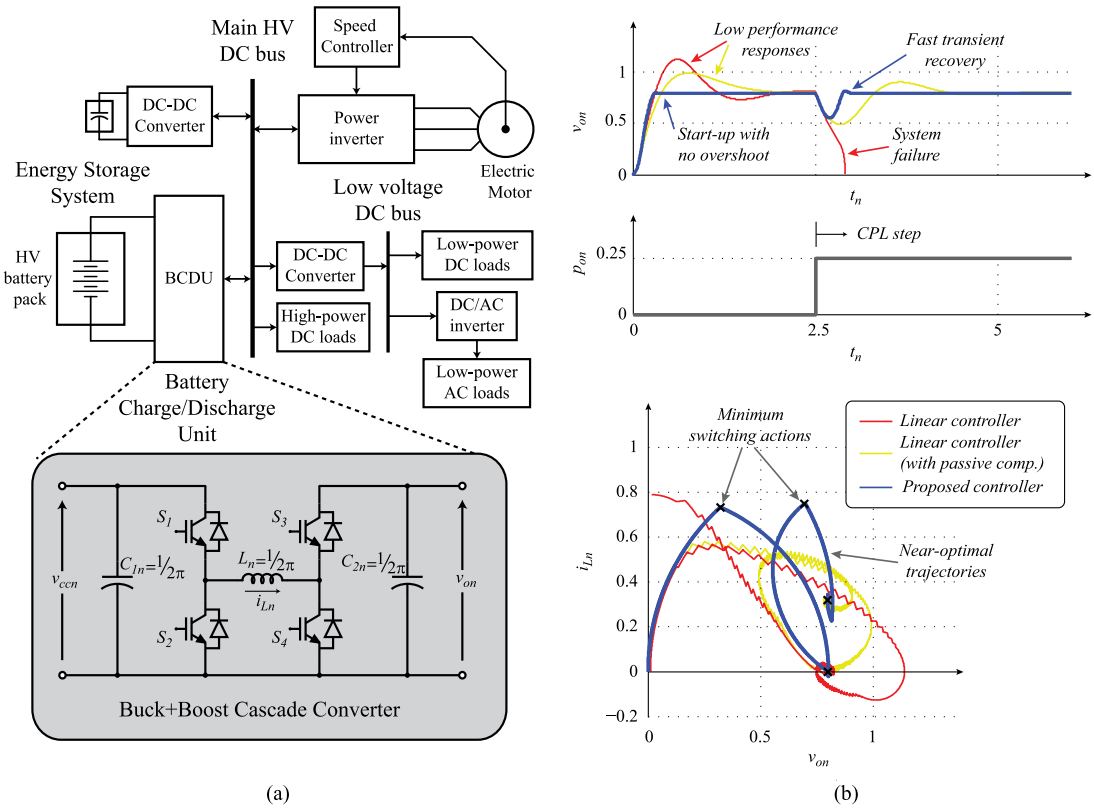

Fig. 1. (a) Simplified block diagram of the electric system of a battery-powered electric car with a Buck + Boost cascade converter implemented as the BCDU. (b) Geometric control implementing the CSS is compared with a traditional linear controller with passive compensation to show the enhanced dynamics of the proposed switching surfaces under CP loading conditions.

expected from tightly regulated downstream converters and drives. The proposed control technique takes into consideration the worst-case scenario of infinite CPL bandwidth as part of the analysis.

Passive stabilization methods were developed to stabilize the open-loop converter by including *RC* and *RL* networks at the resonance frequency of the filter in the converter, increasing the overall damping of the system [14], [15]. Although the method is simple, the addition of elements to the filter reduces the efficiency and penalizes size and cost. Active stabilization methods were presented in [16]–[18] which avoid the introduction of more components. Nevertheless, while these techniques stabilize the open-loop system, feedback controller is still required to achieve system regulation.

Beyond traditional linear controllers, which rely on a linearization process that certainly limits the validity of the controllers to a small area around the operating point, the analysis developed in [19]–[21] demonstrates the potential of nonlinear techniques to address CPL instability. Boundary controllers have been widely studied and have proven to be robust with large-signal validity [22]. Furthermore, with a proper switching surface selection, remarkable improvements can be made in terms of efficiency and dynamic response [23], [24]. This paper proposes a simple and practical nonlinear control implementing circular switching surfaces (CSS) to address CPL instability in cascade dc–dc converters used in electric vehicle power systems. The analysis of switching surfaces in this paper goes beyond typical applications with resistive loading studied in [24] and [25], as well as undamped systems with constant-current loading studied in [26]–[28]. Moreover, it is found that the control technique proposed provides a solution to CP loading conditions, while achieving outstanding dynamic response. Bulky dc-link capacitance employed to provide system stability can be reduced given the improved large-signal stability achieved by the switching surfaces proposed in this paper. This would allow electrolytic capacitors to be replaced by metal-film capacitors; hence, increasing the reliability of the system [29]–[33].

A conceptual comparison between the proposed control technique and a linear controller is illustrated through simulation in Fig. 1(b). The dual-loop linear controller requires compensation for the CPL instability. In this case, passive compensation was provided through an *RC* network. Without compensation, the linear controllers fails to stabilize the output voltage under CPL condition. The results obtained using the proposed switching surfaces show excellent transient behavior over a wide range of operation and provide a theoretical framework that explains the converter dynamics. The predictable behavior of the converter loaded with CPLs is presented by analyzing the system curves in the normalized state plane along with the CSS employed. Simulation and experimental results validate the proposed switching surfaces for CPL operation and confirm the predicted results.

The following section introduces the normalized Buck + Boost cascade converter used for generalizing the development.

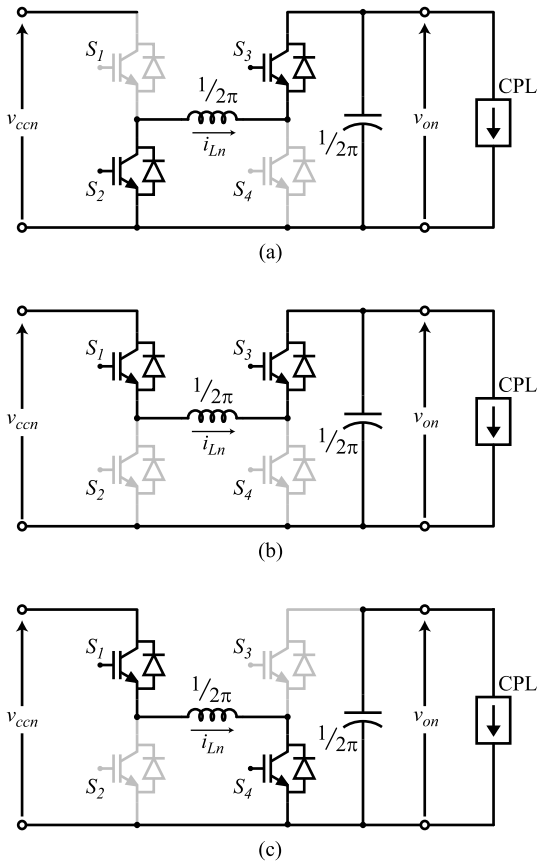

Fig. 2. Normalized Buck + Boost cascade converter structures (a) Structure I $S_2 = S_3 = ON$, (b) Structure II $S_1 = S_3 = ON$, and (c) Structure III $S_1 = S_4 = ON$.

In Section III, the concept of negative impedance of CPLs is briefly reviewed addressing a passive stability criteria and system instability is presented for synchronous and asynchronous operation of the converter. The CSS derivation followed by the closed-loop control technique are presented in Section IV. Section V presents the operating performance of the proposed closed-loop control for startup and sudden load changes. To establish a benchmarking in terms of response improvement, the results obtained are compared with state-of-the-art controllers such as sliding-mode control (SMC) and compensated linear control. Section VI presents the stabilization capabilities and limits of operation. Experimental results obtained in a 1-kW platform are presented in Section VII validating the proposed switching surfaces. Finally, conclusions are stated in Section VIII, remarking the major outcomes of the development and the advantages of the CCS proposed for EV power-system control.

II. Normalized Buck + Boost Cascade Converter

The Buck + Boost cascade converter, shown in Fig. 1(a), is a bidirectional topology obtained by cascading a Buck with a Boost converter, allowing independent step-down or step-up operation. The different structures of the converter are depicted in Fig. 2. In discharge operation (power flow from energy storage to the main dc bus), step-down conversion is obtained by switching between structures I and II. For a step-up operation, structures II and III are employed. The behavior for the converter with CPL is described through the following set of differential equations:

$$L\frac{di_L}{dt} = u_1 v_{cc} - u_2 v_o$$

$$C\frac{dv_o}{dt} = u_2 i_L - \frac{P_o}{v_o}. \tag{1}$$

In (1), u represents the state of the switches: $u_1 = 1$ for switches S_1 and S_2, ON and OFF respectively, and $u_2 = 1$ for switches S_3 and S_4, OFF and ON, respectively.

In order to give generality to the development, the converter is normalized, eliminating dependence on converter voltages, currents, and power ratings as well as filter characteristics

$$v_{xn} = \frac{v_x}{V_{cc}};\;\; i_{xn} = \frac{i_x}{I_{\text{ref}}} = \frac{i_x}{V_{cc}} Z_o;\;\; t_n = \frac{t}{T_0}.$$

The normalization procedure makes use of the following base parameters: the input voltage v_{cc}, characteristic impedance of the combined L and C values $Z_o = \sqrt{L/C}$, and the natural resonance period $T_0 = 2\pi\sqrt{LC}$. The subindex n is used to indicate normalized variables. Normalizing (1) yields the following:

$$\frac{1}{2\pi}\frac{di_{Ln}}{dt_n} = u_1 v_{ccn} - u_2 v_{\text{on}}$$

$$\frac{1}{2\pi}\frac{dv_{\text{on}}}{dt_n} = u_2 i_{Ln} - \frac{P_{\text{on}}}{v_{\text{on}}}. \tag{2}$$

III. Open-Loop Instability

The presence of CPLs in power converters introduces unique dynamics into the system that are not present with typical resistive or constant current loads and which generate open-loop instability in the converter. An ideal CPL can be modeled as (3), where for a given operating point $(V_{\text{on}}, I_{\text{on}})$, the product of the load voltage and current is kept constant constant $(P_{\text{on,const}} = V_{\text{on}} I_{\text{on}})$ and the instantaneous value of the load impedance is positive $(R_{\text{on}} = \frac{V_{\text{on}}}{I_{\text{on}}})$. A linear approximation is obtained by deriving (3) in the small area around $(V_{\text{on}}, I_{\text{on}})$, yielding the linear equivalent incremental impedance R_{eqn}. As shown in (4), R_{eqn} at the given operating point or at any other is negative. The linearized CPL model is (5)

$$i_{\text{on}} = \frac{P_{\text{on}}}{v_{\text{on}}} \tag{3}$$

$$\frac{di_{\text{on}}}{dv_{\text{on}}} = -\frac{P_{\text{on}}}{v_{\text{on}}^2} = -\frac{1}{R_{\text{eqn}}} \tag{4}$$

$$i_{\text{on,lin}} = 2\frac{P_{\text{on}}}{V_{\text{on}}} - \frac{P_{\text{on}}}{V_{\text{on}}^2} v_{\text{on}} = 2I_{\text{on}} - \frac{1}{R_{\text{eqn}}} v_{\text{on}}. \tag{5}$$

A cascade converter in step-down operation mode is illustrated in Fig. 3(a), with normalized inductor and capacitor parasitic resistances included in the model. Considering the converter loaded with a CPL and by using the linearized model (5), small-signal analysis for the input to output transfer function

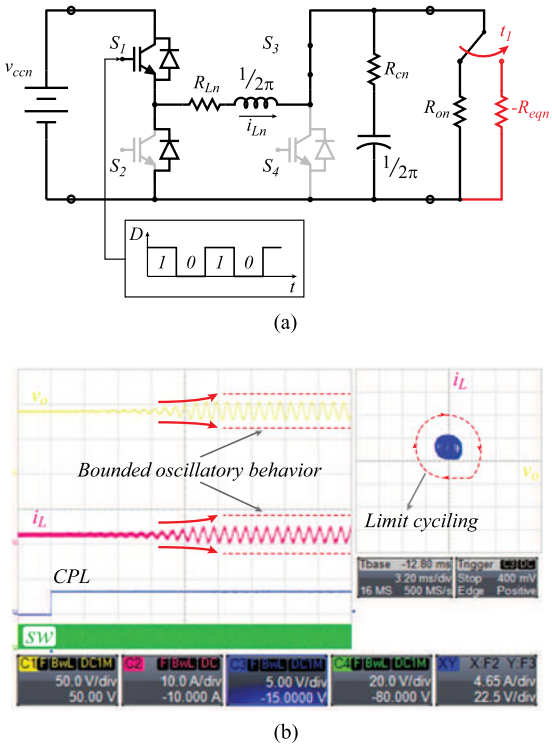

Fig. 3. Bounded oscillatory response is obtained for the open-loop cascade converter in asynchronous step-down operation when load is switched from CR to CP.

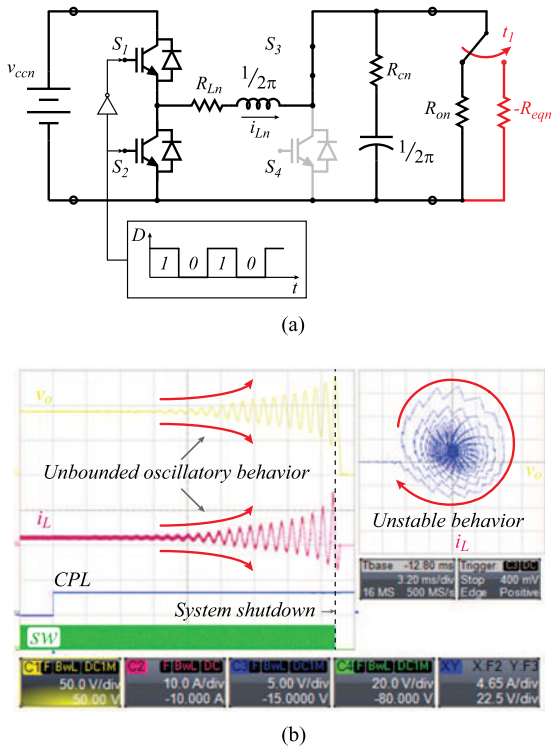

Fig. 4. Unbounded oscillatory response is obtained for the open-loop cascade converter in synchronous step-down operation when load is switched from CR to CP.

yields the following denormalized result:

$$\frac{\hat{v}_o(s)}{\hat{v}_{in}(s)} = \frac{R_{\rm eq}}{R_{\rm eq} - R_c} \frac{1}{s^2\ a + s\ b + c} \tag{6}$$

where

$$a = LC, \quad b = \left[\frac{L}{R_c - R_{\rm eq}} + C\left(R_L + \frac{R_{\rm eq}R_c}{R_{\rm eq} - R_c}\right)\right],$$

$$c = \frac{R_L - R_{\rm eq}}{R_c - R_{\rm eq}}.$$

Analyzing the roots of the characteristic equation in (6), it can be seen that the negative equivalent impedance of the CPL produces a shifting in the system's poles, which may be displaced to the right-half plane, depending on the filter parameters, making the system open-loop unstable. For a high-efficiency converter, the losses R_L and R_c should remain minimal. Thus, stability of the converter relies on oversizing the output capacitance to comply with the following:

$$\frac{L}{\mid R_c - R_{\rm eq} \mid} < C\left(R_L + \frac{R_{\rm eq}R_c}{R_{\rm eq} - R_c}\right). \tag{7}$$

Previous criteria is overly conservative and, as a sufficient condition, it ensures stable operation of the open-loop converter. Figs. 3(b) and 4(b) show the experimental results of the cascade converter operating in open loop in asynchronous and synchronous mode, respectively, with normal capacitor selection (not oversized).

Operation starts with resistive load $R_{\rm on}$ and at $t = 3.2$ ms, the load switches to CP. As expected, the negative incremental impedance has a negative impact on the stability of the system, producing oscillations at the resonance frequency at the output of the converter. With asynchronous operation [see Fig. 3(b)], the load dynamics produce an increase in the energy stored by the reactive elements cycle after cycle, increasing the oscillations until the converter enters into discontinuous conduction mode (DCM). At this point, the inductor current cannot invert the direction and remains discharged while the capacitor continues to discharge. This process limits the energy stored in the reactive elements and the operation quasi-stabilizes after $t \approx 19.2$ ms in a limit cycling, which can be observed in the geometric domain. On the other hand, when switched to synchronous operation [see Fig. 4(b)], inductor current is allowed to reverse direction. Same loading process is applied and in this case, the energy in the reactive elements rises without boundaries, increasing the oscillations until the system is shut down $t \approx 21$ ms using a protection. This unbounded and destructive behavior is a severe concern that will be addressed by the proposed switching surfaces.

Besides the criteria for stable operation derived previously, the combination of CP as well as regular resistive loads in the power system mitigates the CP instability effect. However, the overall system stability should not rely on the existence of such resistive loads. Practical CPLs models differ from (3), mainly due to bandwidth limitations of real converters/inverters acting as loads. In current applications (2014), the bandwidth of the CPLs can range from a few hertz to up to few kilohertz (power supplies connected to the dc link). This study adopts the worst-case operating scenario of ideal CPL, with infinite bandwidth, with the objective of achieving a general control strategy.

As discussed in the following sections, the switching surfaces employed for the control technique allows to obtain near time-optimal solutions irrespective of the bandwidth of the CPL.

IV. CSS-Based Control Strategy

This section presents the derivation of the CCS, which are later employed to define the closed-loop control law for both operating modes.

A. CSS Derivation

To derive the switching surfaces, the normalized differential system (2) is solved to obtained the converter's circular trajectories comprising it's three structures depicted in Fig. 2. The differential equations of the system, repeated in (8), are combined and solved obtaining the time-domain solutions (9) and (10)

$$\begin{aligned}\frac{1}{2\pi}\frac{di_{Ln}}{dt_n} &= u_1 v_{ccn} - u_2 v_{\rm on}\\ \frac{1}{2\pi}\frac{dv_{\rm on}}{dt_n} &= u_2 i_{Ln} - i_{\rm on}\end{aligned} \tag{8}$$

$$\begin{aligned}v_{\rm on} = &\left[v_{\rm on}(0) - \frac{u_1}{u_2}v_{ccn}\right]\cos(2\pi t_n)\\ &+ [u_2 i_{Ln}(0) - i_{\rm on}]\sin(2\pi t_n) + \frac{u_1}{u_2}v_{ccn}\end{aligned} \tag{9}$$

$$\begin{aligned}i_{Ln} = &\left[i_{Ln}(0) - \frac{1}{u_2}i_{\rm on}\right]\cos(2\pi t_n)\\ &+ [u_1 v_{\rm on}(0) - u_2 v_{ccn}]\sin(2\pi t_n) + \frac{1}{u_2}i_{\rm on}.\end{aligned} \tag{10}$$

Combining (9) and (10), time is eliminated obtaining the generalized trajectory as

$$\begin{aligned}\lambda:\ &\left(v_{\rm on} - \frac{u_1}{u_2}v_{ccn}\right)^2 + (u_2 i_{Ln} - i_{\rm on})^2\\ &- \left[v_{\rm on}(0) - \frac{u_1}{u_2}v_{ccn}\right]^2 - [u_2 i_{Ln}(0) - i_{\rm on}]^2 = 0.\end{aligned} \tag{11}$$

Replacing the parameters u_1 and u_2, the trajectories corresponding to each of the structures depicted in Fig. 2 are obtained and shown as

$$\lambda_1:\ v_{\rm on}^2 + (i_{Ln} - i_{\rm on})^2 - v_{\rm on}^2(0) - [i_{Ln}(0) - i_{\rm on}]^2 = 0 \tag{12}$$

$$\begin{aligned}\lambda_2:\ &(v_{\rm on} - v_{ccn})^2 + (i_{Ln} - i_{\rm on})^2\\ &- [v_{\rm on}(0) - v_{ccn}]^2 - [i_{Ln}(0) - i_{\rm on}]^2 = 0\end{aligned} \tag{13}$$

$$\lambda_3:\left(\frac{v_{ccn}}{i_{\rm on}}\right)v_{\rm on} + i_{Ln} - \left(i_{Ln}(0) + \frac{v_{\rm on}(0)\ v_{ccn}}{i_{\rm on}}\right) = 0. \tag{14}$$

These trajectories can be rewritten in the form of

$$\lambda: (x - C_x)^2 + (y - C_y)^2 - \text{radius}^2 = 0 \tag{15}$$

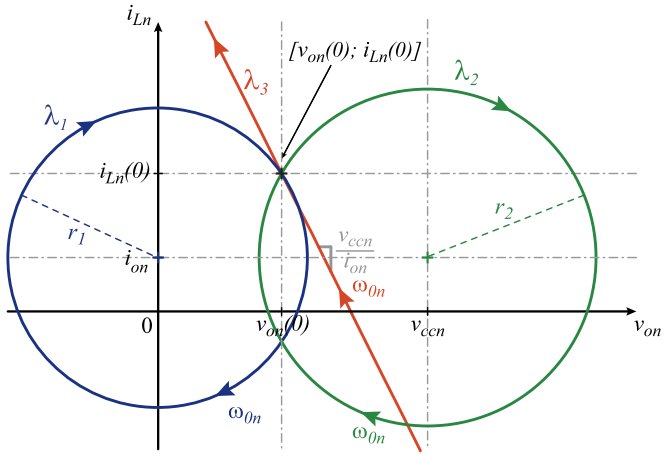

Fig. 5. Buck + Boost cascade converter trajectories, in its three structures, describes circumferences in the state plane.

where the center of the circumferences is displaced by v_{ccn} and $i_{\rm on}$ and the radius depends on the operating point values $v_{\rm on}(0)$ and $i_{Ln}(0)$. To facilitate the visualization, the trajectories λ_1 to λ_3 are illustrated in Fig. 5 for a particular set of parameters $[v_{\rm on}(0), i_{Ln}(0)]$. The direction of the rotational speed $\omega_{\rm on}$ is indicated by a set of arrows on each trajectory. λ_3 is considered a particular case of a circumference in which the center is shifted to $(C_x, C_y) \to (\infty, \infty)$ approaching a straight line in the state plane.

B. Close-Loop Control Law Definition

The trajectories λ_1 to λ_3, defined in the previous section, are employed to define the control law based on the operating point and the intersection of the converters switching surfaces. For this task, some parameters need to be defined. $v_{ccn} = 1$, given that the normalization is done with v_{cc}. $v_{\rm on}(0)$ takes values in an interval $(a < v_{\rm on,target} < b)$, which depends on the battery SOC. The boundaries a and b are given by the maximum and minimum operating values of the energy storage system. The parameter $i_{Ln}(0)$ is matched with the targeted inductor current $(i_{Ln,\rm target})$ for each operating mode. For step-down operation, since structures I and II are used, then $i_{Ln,\rm target} = i_{\rm on}$. For step up, structures II and III are used; hence, i_{Ln} is equal to the input current of the converter and it is related to the output current $i_{\rm on}$ as $i_{Ln,\rm target} = i_{\rm on}/(1 - D)$ with $D = 1 - v_{ccn}/v_{\rm on,target}$. Having all the required parameters defined, the control law is presented for each operating mode.

For step-down operation, $u_2 = 1$ and the control law derived is as follows:

Case I: $(i_{Ln} > i_{\rm on})$
if $(\sigma_1 > 0)$, then $u_1 = 0$, else $u_1 = 1$

Case II: $(i_{Ln} < i_{\rm on})$
if $(\sigma_2 > 0)$, then $u_1 = 1$, else $u_1 = 0$

where

$$\sigma_1:\ v_{\rm on}^2 + (i_{Ln} - i_{\rm on})^2 - V_{\rm on,target}^2 \tag{16}$$

$$\sigma_2:\ (v_{\rm on} - v_{ccn})^2 + (i_{Ln} - i_{\rm on})^2 - (V_{\rm on,target} - 1)^2. \tag{17}$$

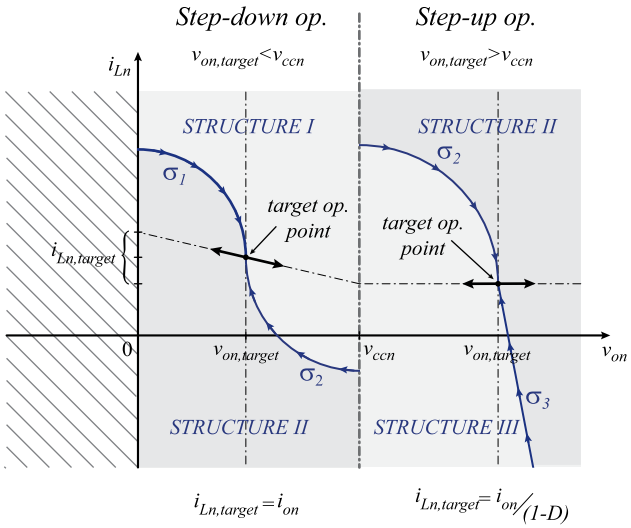

Fig. 6. For closed-loop operation, switching surfaces σ_1 and σ_2 are employed for step-down operation, while σ_2 and σ_3 are used for step-up operation.

In step-up operation, $u_1 = 1$ and the control law is defined as follows:

Case I: $(i_{Ln} > i_{\rm on}/(1-D))$
if $(\sigma_2 > 0)$, then $u_2 = 1$, else $u_2 = 0$

Case II: $(i_{Ln} < i_{\rm on}/(1-D))$
if $(\sigma_3 < 0)$, then $u_2 = 0$, else $u_2 = 1$

where

$$\sigma_2 : (v_{\rm on} - v_{ccn})^2 + (i_{Ln} - i_{\rm on})^2 - (V_{\rm on,target} - 1)^2 - (i_{\rm on}\, V_{\rm on,target} - i_{\rm on})^2 \quad (18)$$

$$\sigma_3 : \left(\frac{1}{i_{\rm on}}\right) v_{\rm on} + i_{Ln} - \left(V_{\rm on,target}\, i_{\rm on} + \frac{V_{\rm on,target}}{i_{\rm on}}\right). \quad (19)$$

Fig. 6 illustrates the control laws with the CSS established, showing the two areas of operation which are determined based on the dynamic value $v_{\rm on,target}$ with respect to v_{ccn}.

To understand the operation and gain insight into the behavior of the CSS-based control strategy proposed, Fig. 7 presents the analysis of the CSS with the converter trajectories loaded with CPL for each structures depicted in Fig. 2. The points A shown in the subfigures correspond to different initial conditions (ICs) for which the CSS have a sufficiently small error regarding the CPL trajectory, ensuring that the target can be achieved by switching to the corresponding structure indicated as $\lambda_{x\_\rm target}$. This condition is satisfied for all the IC that are in the region between the curve $P_{\rm on}$ and a certain limit, which is determined by the maximum output voltage ripple, e.g., 2%. Thus, when the CSS represented as $\lambda_{x\_\rm target}$, within the given region is selected, the trajectories evolve until the condition $v_{\rm on} \pm 2\%$ achieving steady state.

For points B outside the region, where the CSS trajectory matched with the target CPL trajectory, the circles that describe the target CSS trajectory now match with different CPL trajectories that intersect the $p_{\rm on}$ line at a $v_{\rm on}$ value, which can be either higher or lower than $v_{\rm on} = V_{\rm on,target}$ (point A in Fig. 7). However, it can be demonstrated that the operating point always is able to return to the convergence area by switching to the proper structure as it is indicated conceptually in the Fig. 7 for the different cases. Consequently, once point A is reached, the structure is switched according to the operating mode, reaching again the target CSS trajectory that allows to the operating point arrives at the desired target. Although extra switching actions are required, the operating region is extended.

V. Closed-Loop Operation and Performance Assessment

The CSS were implemented in simulation for the Buck + Boost cascade converter for startup and CP loading transients. Results are shown in Fig. 8(a) and (b) for step-down and step-up operation, respectively.

In the first case, the converter is initially driven from ❶ to the target point with no load ❸. With the switches configured as in structure II, the operating point moves along λ_2. When it reaches the switching surface $\sigma_{1(P_{\rm on}=0)}$ ❷, the converter switches to structure I, achieving steady state in two switching actions in minimum time. At instant $t_n = 1$, a CP load of $P_{\rm on} = 0.15$ is applied and the new target point moves to ❺. According to the CSS, the converter switches again to structure II until it reaches the switching surface $\sigma_{1(P_{\rm on}=0.15)}$, where the control now switches back to structure I. The operating point is directed toward the target where it achieves steady state. Same startup and loading process is done for step-up operation and shown in Fig. 8(b). The controller, uses in this case, structures II and III to drive the operating point toward the target with CP load of $P_{\rm on} = 0.2$. These results obtained show the stabilizing capabilities and enhanced transient responses with sudden load changes of the CSS for both operating modes.

Important advantages in terms of performance and switching actions are obtained, when driving the operating point toward the target point through near-optimal trajectories. A comparison between the closed-loop control implementing the CSS with linear compensated control and SMC is shown Fig. 9. Time-domain and state-plane plots show start up and sudden load change transient performance for the three control techniques. The linear controller was implemented in a compensated converter, enabling the use of the normal approach, by analyzing root locus and frequency-domain analysis for the design of the feedback loop. Analyzing the response of the converter to a CPL sudden change, it is observed that the converter achieves stability after 2.32 normalized time units. On the other hand, SMC is an interesting alternative control for stabilizing and controlling CPL systems. For this controller, a transient of 1.15 normalized time unit is obtained for the same load change. With the CSS-based control, the recovery time shown for the same CPL step is 0.34 normalized time units, representing an improvement of 3.4 times with respect to SMC and of 6.8 times with respect to the linear controller. Analyzing the switching actions (in the state-plane plot) required by each technique to arrive to the new target point after the sudden CPL change, it is observed that the proposed controller implements only two switching actions, while for the other two techniques, the number is extremely large.

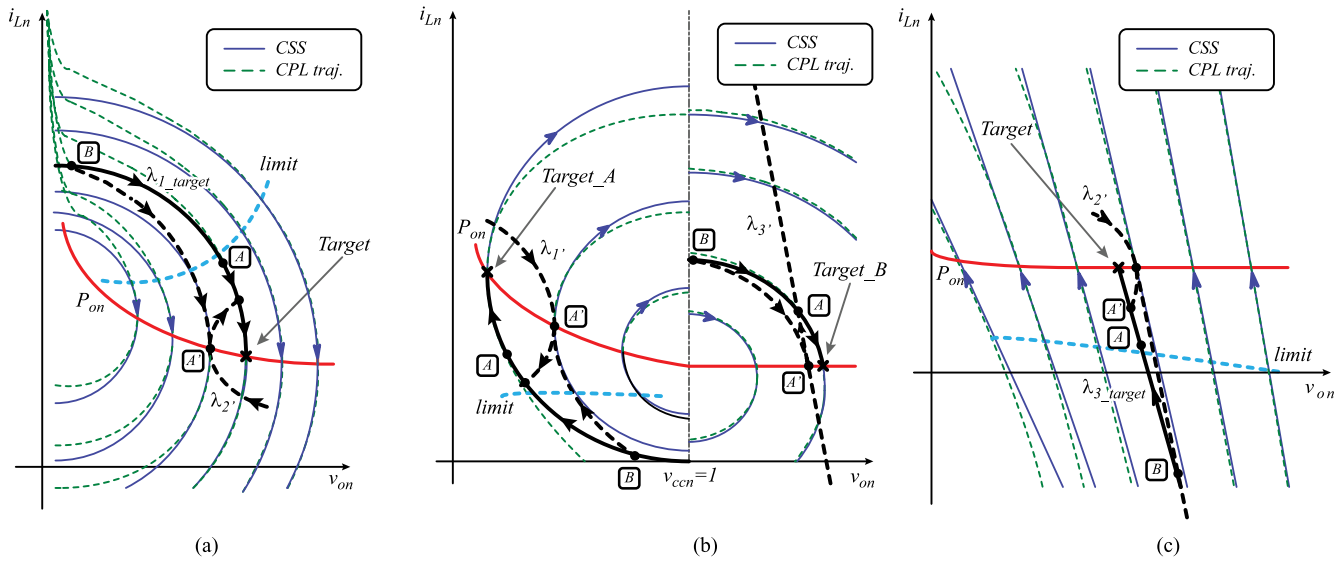

Fig. 7. CSS-based control strategy is conceptually analyzed in the state plane with the CPL trajectories. For the converter in its three structures, a wide operating area is identified for stable operation and optimal transient response.

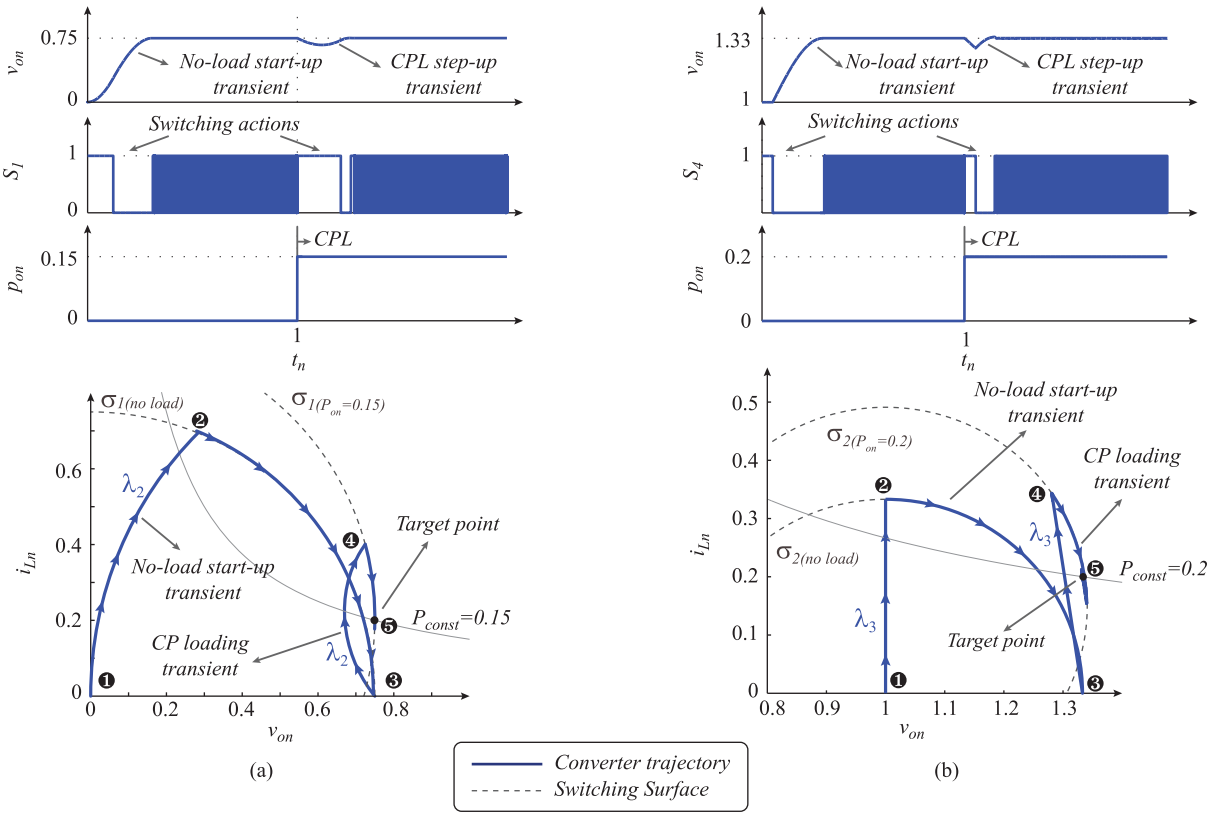

Fig. 8. Closed-loop operation using CSS for (a) step-down and (b) step-up operation. The controller addresses time-optimal start-up and stability operation with near-optimal transient with sudden load changes.

VI. Stability and Limits of Operation

EVs find application in race cars, very high power sport/luxury cars (Tesla S), high torque transportation systems (trucks), heavy duty mining vehicles with extremely high torque, industrial vehicles, and even simple golf carts just to name some applications. As well, there are a number of downstream converters in EV powering systems that imposes high-bandwidth loading conditions. Therefore, the type of CPL loading conditions can range from low bandwidth to very demanding high bandwidth. In particular, the severity of the CPL relates to the transient capability of the power converter. Note that the dynamic response of large power converters is inherently

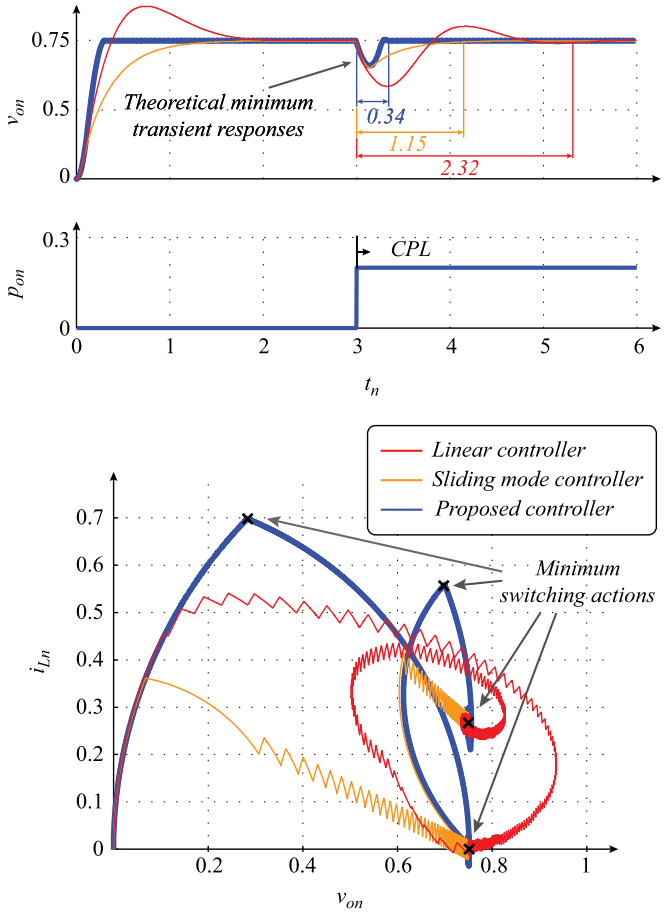

Fig. 9. Simulation results for the proposed closed-loop control based on the CSS shows an important time recovery improvement with reduced switching actions when compared with linear compensated control and SMC.

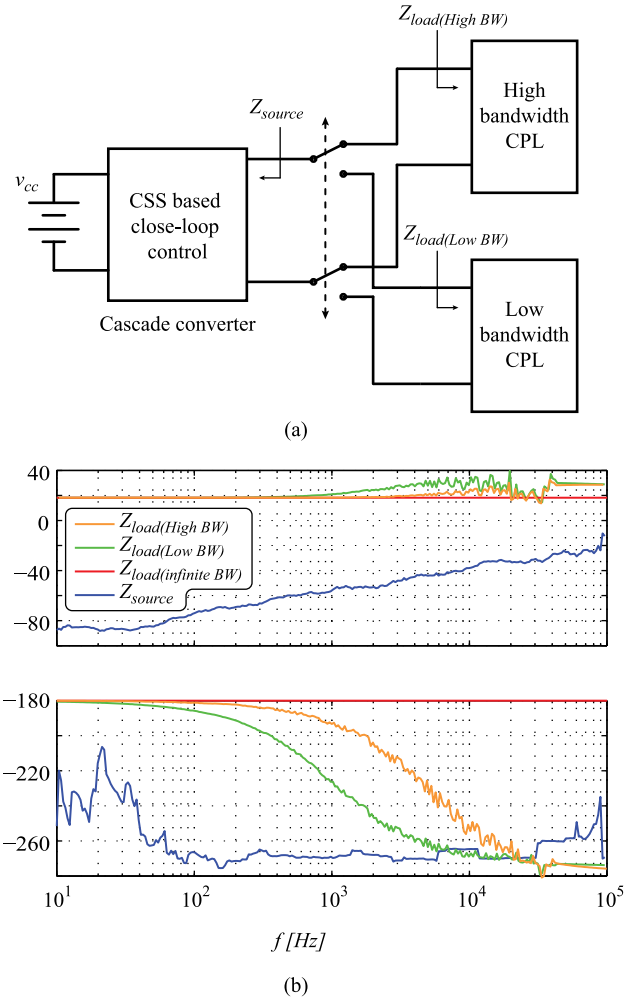

Fig. 10. Impedance analysis results for the structure (a) shown in (b) exhibits a highly reduced Z_{source} for the cascade converter compared with the Z_{load} of the CPLs confirming the stabilization capabilities of the proposed control technique.

limited by the size of the large *LC* filter that restrain the physical transient response. The objective of a good control strategy is to maximize the dynamic response of these converters to compensate for any possible loading condition, even high-bandwidth CPL.

To analyze stabilization capabilities of the proposed control technique, several approaches can be found in the literature. Middlebrook's criterion [34] derived from the impedance ratio analysis in filtered switching power converters is found quite conservative. Nevertheless, combined with gain- and phase-margin criteria, this analysis can deliver good insight into the stabilization characteristics of the controlled converter. In order to study the effect of CPL bandwidth, Fig. 10 shows the output impedance Z_{source} of the cascade converter in closed-loop operation overlapped with the input impedance Z_{load} of three CPL cases. To approach realistic scenarios, two CPLs with a high bandwidth and a limited bandwidth model are considered. The ideal CPL (infinite bandwidth) case is plotted as well, to identify the worst-case scenario. Impedance ratio criterion requires $Z_{\text{source}} << Z_{\text{load}}$, which in practice can be extended to -6-dB difference to ensure stable operation. To this condition, a phase margin of $50°$ is acceptable for stability. As shown in the Bode plot in Fig. 10, CPLs exhibit a negative impedance characteristic. In the case of an ideal CPL (infinite bandwidth), this behavior is extended to the entire frequency range. For the high-bandwidth CPL, this behavior is maintained to up to a frequency of 5 kHz from which the gain starts to increase reducing the instability effects. Variation on the phase also indicates that the behavior is no longer CP type beyond that frequency. For the limited bandwidth CPL, the bandwidth goes up to 500 Hz. On the other hand, the cascade converter (Z_{source}) under study shows a desirable reduced output impedance for a large bandwidth. The bandwidth is enough to ensure stable steady-state operation with both CPL cases even under heavy loading conditions $P_o(\max) = 1$ kW.

To analyze the performance of the proposed switching surfaces, the same three CPL models were implemented in simulation. Results in Fig. 11 show the transient response of the converter with the proposed controller for a low-bandwidth CPL, a high-bandwidth CPL, and finally, an ideal CPL case with infinite bandwidth. The solutions obtained with the proposed switching surfaces for CP loading transient show near time-optimal recovery and stable steady-state operation, even for the worst-case bandwidth scenario. When the bandwidth of

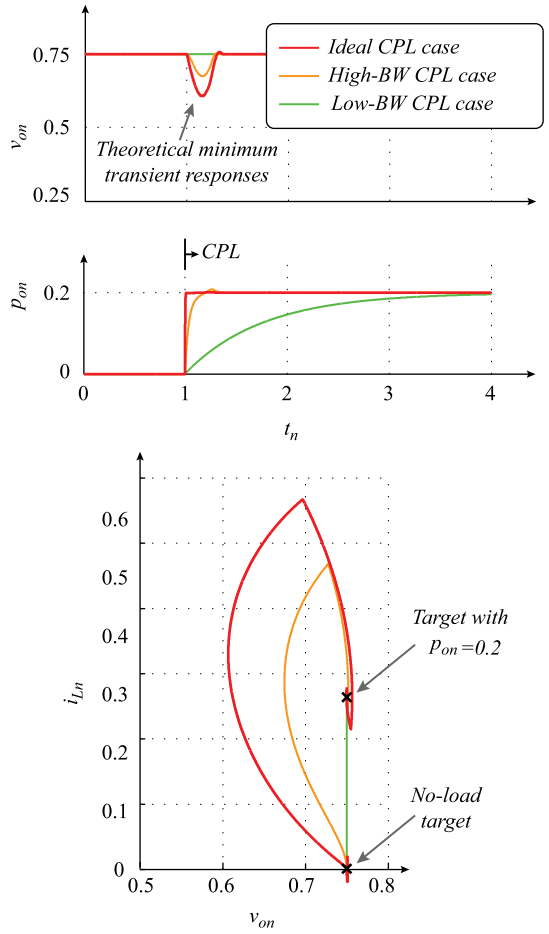

Fig. 11. Simulation results show the time-optimal transient response of the converter with the proposed controller for three cases of CPL in which stable operation is observed for even the worst-case scenario.

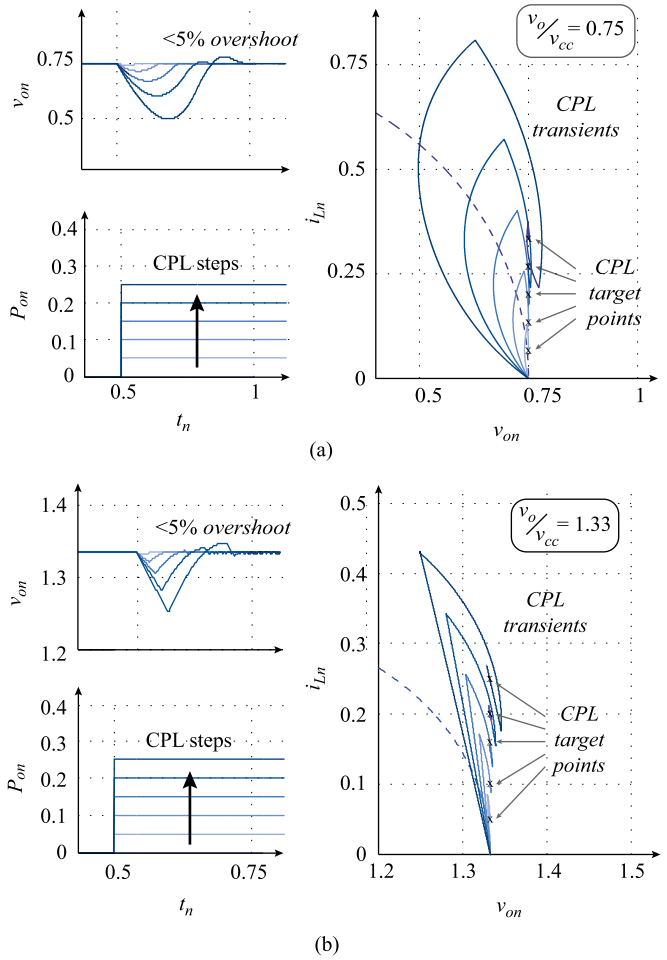

Fig. 12. Transient response for a family CPL steps in (a) step-down operation and (b) step-up operation exhibits the improved response for several loading conditions.

the CPL is limited (low case), the controller is able to regulate the output voltage $v_{\rm on}$ during the loading process without exhibiting a noticeable voltage drop. The corresponding trajectory is a vertical line shown in the state plane plot [see 11(b)]. By increasing the bandwidth of the load to practical levels, the CPL step approaches the ideal step function. As can be observed in the state plane, although the ideal case is more demanding during the loading process, both cases present a near time-optimal recovery using the proposed switching surface.

Moving forward, the analysis and results presented in the previous section can be extended to different operating points along the CP curve, as well as implemented with different CPL steps to characterize the behavior of the proposed controller. Fig. 12 presents the simulation results of the Buck + Boost cascade converter in step-down and step-up operating mode for a family CPL steps. Under the operating conditions indicated in the figure, successive CPLs are applied is steps of $\Delta P_{\rm on} = 0.05$. Curves obtained for the simulation indicate that the controller is able to stabilize CPL steps of up to $P_{\rm on} = 0.25$ for both operating modes exhibiting less than 5% overshoot. These results define an improved dynamic performance over an important set of working conditions making the technique widely applicable for CPL stabilization and loading transient control.

The sensitivity of the control technique regarding filter parameter drifting and tolerances was also examined. Different scenarios were established for the normalization procedure (see Section II, focusing on the filter characteristic impedance $Z_o = \sqrt{L/C}$. The worst case occurs when the value of L or C increases, while the remaining parameter equally decreases. The filter parameters were subject to a variation of 10%. The effect of such variations is the transformation in the switching surfaces, which become elliptical rather than circular. Simulations were developed for the different cases so that the response variations could be analyzed. The distortion of the switching surfaces affects the evolution of the operating point during a sudden load change and showed less than 5% overshoot compared with the ideal case under the same operating conditions. Regarding steady state, the variation observed were negligible. Nevertheless, by applying precise calibration, distortion effect due to parameter variation can be minimized.

VII. Experimental Results

A scaled 1-kW Buck + Boost cascade converter was implemented in hardware with the parameters indicated in Table I. A

TABLE I
CONVERTER PARAMETERS

Parameter	Value
L	920 μH
R_L	0.29 Ω
C	20 μF
ESR	9 mΩ
v_o	90 V
v_{cc}	50 V–200 V
$P_o\,(\max)$	1 kW

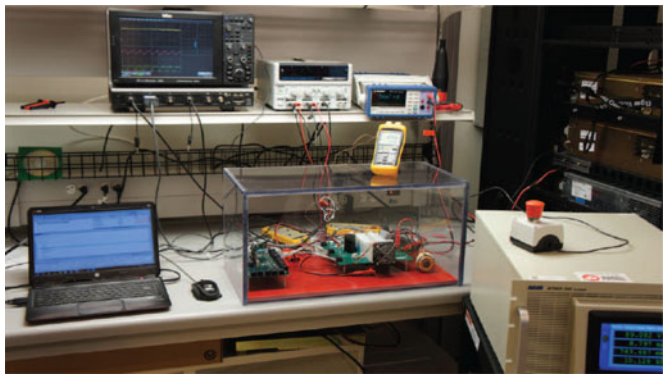

Fig. 13. Cascade converter experimental setup.

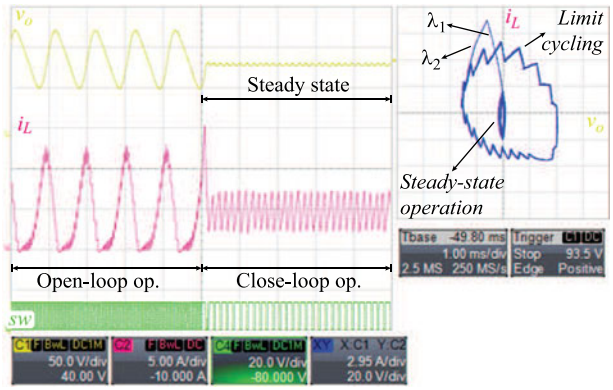

Fig. 14. Output stability experimental results obtained for the converter loaded with 400 W CPL, when operation is switched from open loop to closed loop with the CCS.

fast dynamic CPL with a bandwidth of approximately 25 kHz was implemented as part of the test bench. A picture of the experimental setup is shown in Fig. 13.

For a nominal output power of $P_o = 1$ kW and the filter parameters indicated, the linear stability analysis (7) for traditional controllers indicates that the system is highly unstable. To stabilize the open-loop converter, a 50 times larger electrolytic capacitor (1.1 mF) would be required. This type of capacitor presents an ESR approximately 20 times larger than the ESR of the metal-film type employed, which would certainly increase the losses in the filtering network. For the proposed technique, this enables the usage of metal-film capacitors, which have reliability advantages over commonly employed electrolytic capacitors as well as reduced ESR improving system efficiency. The

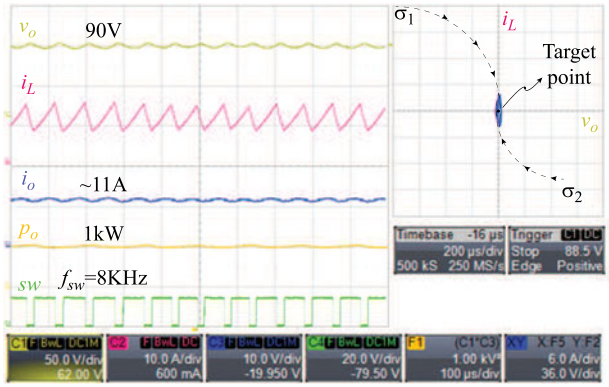

Fig. 15. Experimental results for the cascade converter loaded with 1-kW CPL in closed-loop step-down operation.

open-loop instability concept produced by the CPL is shown in Figs. 3 and 4 (see Section III, where the converter was operating in step-down mode at a fixed switching frequency of $f_{\rm SW} = 20$ kHz and duty cycle $D = 0.75$. The load is initially resistive, dissipating $P_o = 250$ W. The response at the output of the converter after switching to CPL at $t_1 = 3.2$ ms, exhibits oscillatory behavior at the resonance frequency $f_o = 1.15$ kHz. Synchronous operation (see Fig. 4) was identified as the worst-case operating condition, since oscillation grows without boundaries. For protection, output voltage and current thresholds are set to shut down the power stage to avoid a catastrophic failure. If asynchronous switching was to be implemented, operation would be restricted to the first quadrant, thus enabling operation in DCM. In this case, instability effects are reduced by preventing inductor current i_{Ln} from reversing direction and forcing the trajectory to follow the normalized output voltage axis as shown in Fig. 3.

In order to control the unbounded behavior and obtain predictable, stable operation, the proposed CSS was implemented. Experimental results of the converter operating under the control strategy based on the CSS are shown in Figs. 14–17 and in all cases, the experimental results closely resembles the simulation results.

Stabilization of the system under CPL load is shown in Fig. 14, where the converter is loaded with a $P_o = 400$ W CPL. In the first half of the oscilloscope capture, the converter is operating in open loop and exhibits bounded oscillation. The demonstration of the unstable behavior is done in asynchronous mode to limit the amplitude of the oscillations in open loop. In the second half of the oscilloscope capture, the proposed CSS strategy is enabled, resulting in stable operation. Note that the controller only performs two switching actions (structures I and II) to drive the operating point toward the target point where it remains stable.

In Fig. 15, the converter's stability is further tested by loading the converter with $\mathrm{P_o\,(max)} = 1$ kW. The converter exhibits stable operation with a switching frequency of $f_{\rm SW} = 8$ kHz, which is accomplished by employing an hysteresis band in the CSS control laws to obtain the desired ripple. As for frequency shifting, a narrow variation is observed in steady-state operation. If necessary, this variation can be further mitigated by adjusting

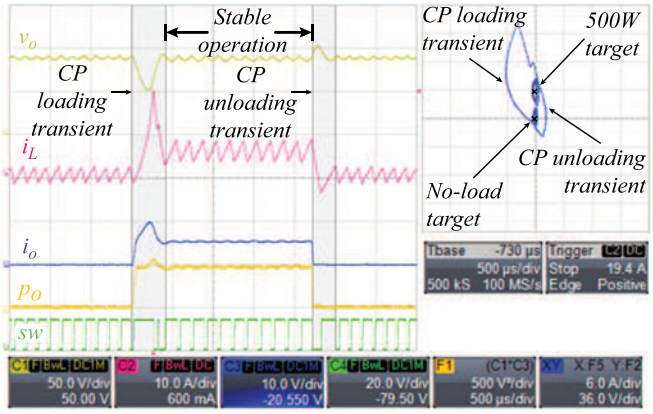

(a)

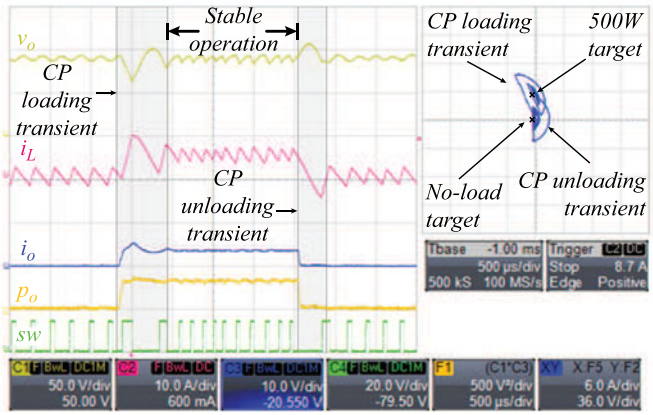

(b)

Fig. 16. Experimental results in the 1-kW platform in (a) step-down operation and (b) step-up operation for a 500-W CPL loading and unloading conditions, exhibiting the near-optimal operation with the CSS control strategy.

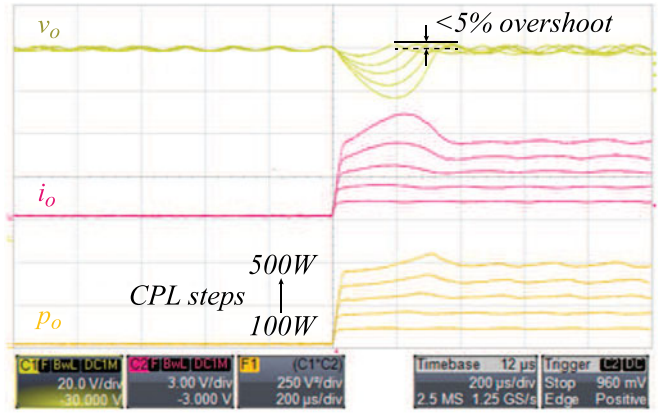

(a)

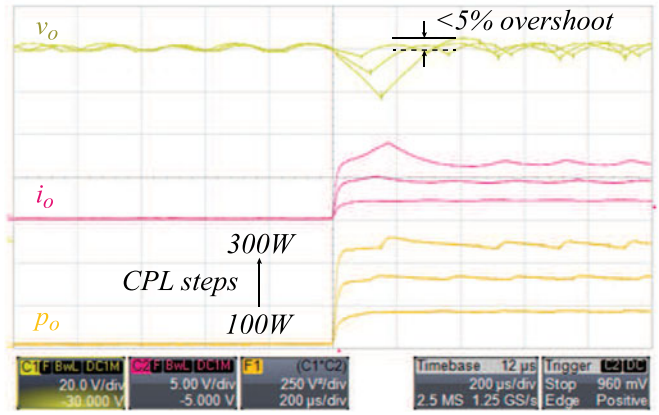

(b)

Fig. 17. Experimental results in the 1-kW platform in (a) step-down and (b) step-up operation for several CPL steps show improved dynamic output response with minimum overshoot.

the hysteresis band control in the CSS or forcing PWM triggering with precision timers.

Experimental results for transient response to CPL sudden change were shown in Fig. 16 for step-down and step-up operating modes. State plane figure on the right-hand side of each experimental capture exposes the evolution of the operating point, through near optimal trajectories, from no-load steady state to a 500-W CP loading condition. Unloading to no-load condition is exercised as well for both cases obtaining the same result in terms of transient recovery.

Further experimental results to evaluate the predicted transient response are shown in Fig. 17(a) and (b), where a family CPL sudden step changes are applied to converter. In Fig. 17(a), the cascade converter is operating in step-down mode with $V_o/V_{cc} = 0.75$. While regulating at 90 V, the CPL step-ups are applied and in each case the control strategy responds by changing the converter structures according to the CSS control law, achieving fast recovery to steady state. The results exhibit an output voltage overshoot of less than 5% for CPLs up to $P_o(\max) = 500$ W as was predicted in Section VI. Fig. 17(b) shows near-optimal response for a CPL sudden load change with negligible overshoot for the cascade converter operating at $V_o/V_{cc} = 1.25$ (step-up operation).

VIII. Conclusion

The CSS was proposed for controlling the BCDU in EV systems in order to mitigate the instability created by CPLs. This simple and practical geometric technique presented the solution for challenging combination high-bandwidth CPL and unbounded oscillation due to synchronous operation of the converter, and yielded large-signal stability and enhanced dynamic transient response over a wide range of operating conditions. Comparison with state-of-the-art linear and nonlinear controllers showed a transient recovery improvement of up to 3.4 times and a considerable reduction in switching actions, thereby improving efficiency. The control laws based on the CSS were derived from a normalized converter generalizing the application. Furthermore, the analysis led to a theoretical framework in which predictable transient performance can be achieved.

The application of this control technique enables a reduction in the size of the bulky dc-link capacitance usually employed to stabilize the main bus. This allows the usage of metal-film capacitors, which have reliability advantages over commonly employed electrolytic capacitors, as well as reduced ESR improving system efficiency. Experimental results developed in a

1-kW Buck + Boost cascade converter validated the concepts described and the application of the CCS for CPL transient rejection and steady-state stable operation.

REFERENCES

[1] A. Emadi, M. Ehsani, and J. M. Miller, "Automotive power systems," in *Vehicular Electric Power Systems: Land, Sea, Air, and Space Vehicles.* New York, NY, USA: Marcel Dekker, Dec. 2003.

[2] Z. J. Shen, "Optimal power management and distribution in automotive systems," in *Handbook of Automotive Power Electronics and Motor Drives*, A. Emadi Ed. Boca Raton, FL, USA: CRC Press, 2005.

[3] A. Emadi, S. S. Williamson, and A. Khaligh, "Power electronics intensive solutions for advanced electric, hybrid electric, and fuel cell vehicular power systems," *IEEE Trans. Power Electron.*, vol. 21, no. 3, pp. 567–577, May 2006.

[4] O. Hegazy, R. Barrero, J. Van Mierlo, P. Lataire, N. Omar, and T. Coosemans, "An advanced power electronics interface for electric vehicles applications," *IEEE Trans. Power Electron.*, vol. 28, no. 12 pp. 5508–5521, Dec. 2013.

[5] A. Khaligh, "Stability criteria for the energy storage bi-directional Dc/Dc converter in the toyota hybrid system II," in *Proc. IEEE Veh. Power Prop. Conf.*, Sep. 2007, pp. 348–352.

[6] S. Waffler and J.W. Kolar, "A novel low-loss modulation strategy for high-power bidirectional Buck + Boost converters," *IEEE Trans. Power Electron.*, vol. 24, no. 6, pp. 1589–1599, Jun. 2009.

[7] R. M. Schupbach and J. C. Balda, "Comparing DC-DC converters for power management in hybrid electric vehicles," in *Proc. IEEE Electr. Mach. Drives Conf.*, Jun. 2003, vol. 3, pp. 1369–1374.

[8] F. Caricchi, F. Crescimbini, F. Giulii Capponi, and L. Solero, "Study Of Bi-Directional Buck-Boost Converter Topologies For Application In Electrical Vehicle Motor Drives," in *Proc. IEEE Appl. Power Electron. Conf.*, Feb. 1998, vol. 1, pp. 287–293.

[9] F. Caricchi, F. Crescimbini, G. Noia, and D. Pirolo, "Experimental study of a bidirectional dc-dc converter for the dc link voltage control and regenerative braking in PM motor drives devoted to electrical vehicles," in *Proc. IEEE Appl. Power Electron. Conf.*, Feb. 1994, vol. 1, pp. 381–386.

[10] F. Caricchi, F. Crescimbini, A. Di Napoli, and M. Marcheggiani, "Prototype of electric vehicle drive with twin water-cooled wheel direct drive motors," in *Proc. IEEE Power Electron. Spec. Conf.*, Jun. 1996, pp. 1926–1932.

[11] Y. A.-R. I. Mohamed, A. A. A. Radwan, and T. K. Lee, "Decoupled reference-voltage-based active DC-link stabilization for PMSM drives with tight-speed regulation," *IEEE Trans. Ind. Electron.*, vol. 59, no. 12, pp. 4523–4536, Dec. 2012.

[12] X. Y. Liu and A. J. Forsyth, "Comparative study of stabilizing controllers for brushless DC motor drive systems," in *Proc. IEEE Electr. Mach. Drives Conf.*, May 2005, pp. 1725–1731.

[13] A. Emadi, A. Khaligh, C. H. Rivetta, and G. A. Williamson, "Constant power loads and negative impedance instability in automotive systems: Definition, modeling, stability, and control of power electronic converters and motor drives," *IEEE Trans. Veh. Technol.*, vol. 55, no. 4, pp. 1112–1125, Jul. 2006.

[14] A. M. Rahimi and A. Emadi, "An analytical investigation of DC/DC power electronic converters with constant power loads in vehicular power systems," *IEEE Trans. Veh. Technol.*, vol. 58, no. 6, pp. 2689–2702, Jul. 2009.

[15] M. Cespedes, Lei Xing, and Jian Sun, "Constant-power load system stabilization by passive damping," *IEEE Trans. Power Electron.*, vol. 26, no. 7, pp. 1832–1836, Jul. 2011.

[16] A. M. Rahimi and A. Emadi, "Active damping in DC/DC power electronic converters: A novel method to overcome the problems of constant power loads," *IEEE Trans. Ind. Electron.*, vol. 56, no. 5, pp. 1428–1439, May 2009.

[17] A. M. Rahimi, G. A. Williamson, and A. Emadi, "Loop-cancellation technique: A novel nonlinear feedback to overcome the destabilizing effect of constant-power loads," *IEEE Trans. Veh. Technol.*, vol. 59, no. 2, pp. 650–661, Feb. 2010.

[18] P. Magne, B. Nahid-Mobarakeh, and S. Pierfederici, "General active global stabilization of multiloads DC power networks," *IEEE Trans. Power Electron.*, vol. 275, no. 4, pp. 1788–1798, Apr. 2012.

[19] C. N. Onwuchekwa and A. Kwasinski, "Analysis of boundary control for buck converters with instantaneous constant-power loads," *IEEE Trans. Power Electron.*, vol. 25, no. 8, pp. 2018–2032, Aug. 2010.

[20] C. N. Onwuchekwa and A. Kwasinski, "Analysis of boundary control for boost and buck-boost converters in distributed power architectures with constant-power loads," in *Proc. IEEE Appl. Power Electron. Conf.*, Mar. 2011, pp. 6–11.

[21] Y. Zhao, W. Qiao, and D. Ha, "A sliding-mode duty-ratio controller for DC/DC Buck converters with constant power loads," *IEEE Trans. Ind. Appl.*, vol. 50, no. 2, pp. 1448–1458, Mar./Apr. 2014.

[22] R. Munzert and P. T. Krein, "Issues in boundary control [of power convertors]," in *Proc. IEEE Power Electron. Spec. Conf.*, Jun. 1996, pp. 810–916.

[23] M. Ordonez, M. T. Iqbal, and J. E. Quaicoe, "Selection of a curved switching surface for buck converters," *IEEE Trans. Power Electron.*, vol. 21, no. 4, pp. 1148–1153, Jul. 2006.

[24] K. K. S. Leung and H. S.-H. Chung, "Derivation of a second-order switching surface in the boundary control of buck converters," *IEEE Power Electron. Lett.*, vol. 2, no. 2, pp. 63–67, Jun. 2004.

[25] T. Siew-Chong, Y. M. Lai, C. K. Tse, and M. K. H. Cheung, "A fixed-frequency pulse width modulation based quasi-sliding-mode controller for buck converters," *IEEE Trans. Power Electron.*, vol. 20, no. 6, pp. 1379–1392, Nov. 2005.

[26] J. M. Galvez, M. Ordonez, F. Luchino, and J. E. Quaicoe, "Improvements in boundary control of boost converters using the natural switching surface," *IEEE Trans. Power Electron.*, vol. 26, no. 11, pp. 3367–3376, Nov. 2011.

[27] M. Ordonez, J. E. Quaicoe, and M. T. Iqbal, "Advanced boundary control of inverters using the natural switching surface: Normalized geometrical derivation," *IEEE Trans. Power Electron.*, vol. 23, no. 6, pp. 2915-2930, Nov. 2008.

[28] G.G. Oggier, M. Ordonez, J. M. Galvez, and F. Luchino, "Fast transient boundary control and steady-state operation of the dual active bridge converter using the natural switching surface," *IEEE Trans. Power Electron.*, vol. 29, no. 2, pp. 946–957, Feb. 2014.

[29] M. Salcone and J. Bond, "Selecting film bus link capacitors for high performance inverter applications," in *Proc. IEEE Electr. Mach. Drives Conf.*, May 2009, pp. 1692–1699.

[30] L. Gu, X. Ruan, M. Xu, and K. Yao, "Means of eliminating electrolytic capacitor in AC/DC power supplies for LED lightings," *IEEE Trans. Power Electron.*, vol. 24, no. 5, pp. 1399–1408, May 2009.

[31] K. Yao, X. Ruan, X. Mao, and Z. Ye, "Reducing storage capacitor of a DCM Boost PFC converter," *IEEE Trans. Power Electron.*, vol. 27, no. 1, pp. 151–160, Jan. 2012.

[32] T. Messo, J. Jokipii, J. Puukko, and T. Suntio, "Determining the value of DC-link capacitance to ensure stable operation of a three-phase photovoltaic inverter,"*IEEE Trans. Power Electron.*, vol. 29, no. 2, pp. 665–673, Feb. 2014.

[33] H. Wang, H. S.-H. Chung, and W. Liu, "Use of a series voltage compensator for reduction of the DC-link capacitance in a capacitor-supported system," *IEEE Trans. Power Electron.*, vol. 29, no. 3, pp. 1163–1175, Mar. 2014.

[34] R. D. Middlebrook, "Input filter considerations in design and application of switching regulators," in *Proc. IEEE Ind. Appl. Soc. Annu. Meet.*, 1976, pp. 366–382.

Matias Anun (S'12–M'14) was born in Cordoba, Argentina. He received the Ing. degree in electronics engineering from the National University of Cordoba, Cordoba, Argentina, in 2010, and the M.A.Sc. degree in electrical and computer engineering from the University of British Columbia, Vancouver, BC, Canada, in 2014.

He is currently a Firmware Engineer with Schneider Electric Solar Business, Burnaby, BC. His experience includes the development of embedded systems and firmware at the Aeronautic University Institute, Argentina and research on electric vehicle power converters and control at the University of British Columbia, Canada.

Mr. Anun as a student received numerous scholarships and awards including a research scholarship granted by the Ministry of Defense, Applied Research Center, Aeronautic University Institute, Argentina, in 2010, and the Top #1 Electronics Engineering Student Granted by the Professional Association of Engineers of Cordoba, National University of Cordoba, Argentina, in 2010.

Martin Ordonez (S'02–M'09) was born in Neuquen, Argentina. He received the Ing. degree in electronics engineering from the National Technological University, Cordoba, Argentina, in 2003, and the M.Eng. and Ph.D. degrees in electrical engineering from the Memorial University of Newfoundland (MUN), St. John's, NL, Canada, in 2006 and 2009, respectively.

He is currently an Assistant Professor with the Department of Electrical and Computer Engineering, University of British Columbia, Vancouver, BC, Canada. He is also a Canada Research Chair in Power Converters for Renewable Energy Systems, as well as an Adjunct Professor with Simon Fraser University, Burnaby, BC, and MUN. His industrial experience in power conversion includes research and development at Xantrex Technology Inc./Elgar Electronics Corp., currently AMETEK Programmable Power in San Diego, CA, USA, Deep-Ing. Electronica de Potencia, Rosario, Argentina, and TRV Dispositivos, Cordoba, Argentina. With the support of industrial funds and the Natural Sciences and Engineering Research Council, he has contributed more than 60 publications and R&D reports.

Dr. Ordonez is an Associate Editor of the IEEE TRANSACTIONS ON POWER ELECTRONICS, serves on several IEEE committees, and reviews widely for IEEE/IET journals and international conferences. He received the David Dunsiger Award for Excellence in the Faculty of Engineering and Applied Science in 2009 and the Chancellors Graduate Award/Birks Graduate Medal in 2006. He is a Fellow of the School of Graduate Studies, MUN.

Ignacio Galiano Zurbriggen (S'11) was born in San Francisco, Cordoba, Argentina. He received the Ing. degree in electronics engineering from the National University of Cordoba, Cordoba, in 2010, and the M.A.Sc. degree from the University of British Columbia, Vancouver, BC, Canada, in 2013, where he is currently working toward the Ph.D. degree.

His work in power electronics includes industrial experience at COMPUTROL Ingeniera Electronica, San Francisco, where he designed and implemented power conversion platforms and digital controllers. His current research interests include the study of linear, nonlinear (geometric), and mixed control strategies for power electronic converters applied to renewable energy systems.

Mr. Zurbriggen has received numerous awards and scholarships including the Faculty of Applied Science Graduate Awardby the University of British Columbia in 2014, the School of Graduates Studies Fellowship by the Memorial University of Newfoundland in 2011, declined, and several undergraduate academic excellence awards by the National University of Cordoba in 2010.

German G. Oggier (M'10) was born in Cordoba, Argentina. He received the Electr. Eng. degree and the M.Sc. degree in electrical engineering from the Universidad Nacional de Rio Cuarto, Rio Cuarto, Argentina, in 2003 and 2006, respectively, and the Doctor degree in control systems from the Universidad Nacional del Sur, Buenos Aires, Argentina, in 2009.

He was a Postdoctoral Fellow with Simon Fraser University, Metro Vancouver, BC, Canada, during 2011 to 2012 and with the University of British Columbia, Vancouver, in 2014. His Postdoctoral research activities include the area of boundary control of power converters. He is currently a Lecturer in the Grupo de Electronica Aplicada, Universidad Nacional de Rio Cuarto. He is also a Researcher with the Consejo Nacional de Investigaciones Cientificas y Tecnicas (CONICET), Buenos Aires, Argentina. His current research interests include power electronics, electric vehicles, and renewable energy conversion.